journal

J. Am. Ceram. Soc., 89 [6] 1965–1971 (2006)
DOI: 10.1111/j.1551-2916.2006.01049.x

Texture Measurements in ⟨001⟩ Fiber-Oriented PMN–PT

Kristen H. Brosnan*,† and Gary L. Messing*

Department of Materials Science & Engineering and the Materials Research Institute, Pennsylvania State University, University Park, Pennsylvania 16802

Richard J. Meyer, Jr.

The Applied Research Laboratory, Pennsylvania State University, University Park, Pennsylvania 16802

Mark D. Vaudin*

National Institute of Standards and Technology, Ceramics Division, Gaithersburg, Maryland 20899

Textured (1-*x*)($Mg_{1/3}Nb_{2/3}$)O_3–*x*$PbTiO_3$ (PMN–PT) ceramics obtained by the templated grain growth process possess a significant fraction of the piezoelectric properties of Bridgman-grown single crystals at a fraction of the cost. However, for integration of these materials into transducer and actuator designs, a more comprehensive characterization of texture quality than possible with Lotgering analysis is needed. In this study, X-ray diffraction (XRD) and electron backscatter diffraction techniques were used to characterize the fiber texture in ⟨001⟩-oriented PMN–28PT. The March–Dollase equation was fitted to the intensity data to describe the texture in terms of the texture fraction, *f*, and the degree of texture of the oriented fraction using the March parameter, *r*. Although each of the techniques used was quantitatively in agreement, XRD rocking curve collection and analysis was the most time-efficient technique for making a comprehensive measurement of texture ($f = 0.69$, $r = 0.29$, FWHM = 13.9°) for fiber-oriented PMN–28PT.

I. Introduction

SINGLE crystals of lead magnesium niobate–lead titanate, (1-*x*)$Pb(Mg_{1/3}Nb_{2/3})O_3$–*x*$PbTiO_3$ (PMN–PT) with compositions close to the morphotropic phase boundary, when cut, oriented, and measured in the ⟨001⟩ direction, have demonstrated a high saturation strain, a high piezoelectric coefficient ($d_{33} > 1500$ pC/N), and a high longitudinal electromechanical coupling coefficient ($k_{33} > 0.90$).[1–3] Single-crystal PMN–PT shows a higher strain than soft lead zirconate titanate (PZT) and less hysteresis than hard PZT, making the single crystal ideal for actuator- and transducer-type applications.[3] Currently, the Bridgman method is used to produce single-crystal PMN–PT of appropriate size for actuator and transducer applications. This method can produce crystals on the order of 30 mm diameter and 150 mm length.[1,4] Bridgman-grown PMN–PT crystals have a chemical heterogeneity of Ti^{+4} along the length of the boule.[5] Because of the sensitivity of the piezoelectric properties to composition, the chemical inhomogeneity renders a large fraction of the Bridgman grown single crystals unusable.

While Bridgman PMN–PT single crystals are limited by production cost, size, and compositional uniformity, textured ceramics can be processed by tape casting, a common cost-effective commercial technique that has a high yield. Textured PMN–32.5PT obtained by the templated grain growth (TGG) process has been shown to possess a significant fraction of the piezoelectric properties of Bridgman-grown single crystals.[6–11] The TGG process allows for the development of a crystallographic texture in polycrystalline ceramics by grain growth of aligned template particles. For example, Sabolsky *et al.* used $BaTiO_3$ templates to produce fiber-textured (anisotropic in the ⟨001⟩ direction) PMN–32.5PT. Textured samples with a 0.82 Lotgering factor (a texture characterization technique that compares the relative X-ray peak intensities) displayed 0.32% strain at 45 kV/cm and a unipolar (<10 kV/cm) piezoelectric coefficient (d_{33}) of 1200 pC/N to 1400 pC/N. Although Sabolsky *et al.* showed enhanced piezoelectric, electromechanical coupling, and compliance coefficients, texturing PMN-32.5PT ceramics with large (100–300 μm) $BaTiO_3$ templates resulted in extremely coarse microstructures (textured grain size >100 μm) and thus too low a strength for most actuator and transducer applications.[6,7,9]

Kwon *et al.*[10] results also showed enhanced piezoelectric properties for PMN–32.5PT in which the fiber texture had been produced using $SrTiO_3$ platelets. Kwon *et al.*[10] reported a Lotgering factor ≈0.70 in high-density PMN–PT. These materials had high strain (>0.30% at 50 kV/cm) and high d_{33} coefficients (>1600 pC/N at <5 kV/cm).

To evaluate accurately the performance of these materials in device applications, a more comprehensive characterization of texture quality is needed. This is illustrated by the impact of misorientation on the piezoelectric response in single crystals. Park and Shrout[3] showed that for 0.955$Pb(Zn_{1/3}Nb_{2/3})O_3$–0.045$PbTiO_3$ single crystals, the unipolar piezoelectric response is halved for a 20° miscut from the ⟨001⟩. Understanding the degree of misorientation of textured grains can lead to more innovative methods for processing of textured materials, and thus a better piezoelectric response in these materials.

To date, only Lotgering analysis has been used to characterize texture in fiber-oriented PMN–PT. The Lotgering method is a comparison of relative X-ray peak intensities of the 00*l* reflections with all of the observed reflections in the spectrum, where random orientation is 0 and fully textured is 1.[6–10,12–14] While the Lotgering factor can be easily measured, it is only a semi-quantitative estimate of the degree of texture. The Lotgering method yields no quantitative information about the degree of misorientation of grains or textured volume fraction, but it is a useful quality factor that allows the development of texture in a series of structurally similar materials to be qualitatively evaluated. Thus, the Lotgering method is insufficient for the compre-

D. Green—contributing editor

Manuscript No. 21347. Received January 7, 2006; approved February 22, 2006.
Presented at the 9th International Ceramic Processing Science Symposium, Coral Springs, FL, January 11, 2006 (Microstructure Control, Paper No. ICPSS-147-2006).
Research supported by the Office of Naval Research, YIP, N00014-03-1-0481 and the Applied Research Laboratory Exploratory and Foundational Research Program.
*Member, American Ceramic Society.
†Author to whom correspondence should be addressed. e-mail: khb115@psu.edu

hensive characterization of texture needed for materials incorporated into devices. Furthermore, there is recent evidence that the texture factor given by the Lotgering method is dependent on the number of reflections used in the calculation and can be misleading.[15] For these reasons, textured materials need to be well characterized by both the fraction of oriented material and by the degree of orientation.

Other X-ray diffraction (XRD) techniques such as pole figures and rocking curves give quantitative information about the orientation distribution in textured alumina and in textured piezoelectric ceramics. The orientation data can be fitted with a texture model such as the March–Dollase equation to determine the fraction of oriented material (f) and the degree of orientation (r) of the material.[16–18] Recently, electron backscatter diffraction (EBSD) has also been utilized for texture characterization in other piezoelectric materials such as $Na_{0.5}Bi_{0.5}TiO_3$–$BaTiO_3$ and for the analysis of PMN–35PT single crystals grown by seeded polycrystal conversion.[18,19]

In this paper, the XRD Lotgering method, stereographic analysis, rocking curves, pole figures, and EBSD were utilized to characterize the crystallographic texture orientation distribution in fiber-oriented PMN–28PT. The March–Dollase equation was used to model the orientation distribution from XRD rocking curve and EBSD data, and texture was quantified in terms of f and r.

II. Experimental Procedure

A precursor mixture of $0.72Pb(Mg_{1/3}Nb_{2/3})O_3$–$0.28PbTiO_3$ (PMN–28PT) was prepared using $(PbCO_3)_2Pb(OH)_2$ (mean particle size of 3.01 μm; Aldrich Chemical Co., Milwaukee, WI), $MgNb_2O_6$ (mean particle size of 1.91 μm, H.C. Starck Inc., New York, NY), and fumed TiO_2 (mean particle size of 20 nm, Degussa Hüls, Frankfurt, Germany). The mean particle sizes of precursors were measured by laser light scattering and by Field Emission Scanning Electron Microscopy (FESEM).

The precursor powders were ball milled for up to 5 days with high-purity ZrO_2 milling media (3 mm diameter). After milling, the mean particle size was measured by laser light scattering. The slurries were dried on a hot plate while stirring and then sieved to <90 μm (170 mesh). Fine precursor powder (mean particle size 0.60 μm) was calcined in a covered crucible for 1 h at 700°C to form the perovskite phase. The calcined powder was sieved to <90 μm (170 mesh). The precursor was ball milled with toluene, an organic binder (Ferro 73210, Vista, CA), and a modifier (Ferro 1111) for 1 day. Five percent by volume fraction tabular $SrTiO_3$ single crystals (NexTech Materials, Ltd., Lewis Center, OH) with a high aspect ratio (thickness, $t = 2$–5 μm and diameter, $d = 20$–40 μm) were added to the slurry by mixing with a magnetic stir bar. The $SrTiO_3$ templates, with $\langle 001 \rangle$ in the thickness direction, were synthesized by a two-step molten salt process using a KCl flux.[20,21] Tapes were cast at 200 μm doctor blade height and a speed of 60 cm/min to orient the templates in the PMN–PT matrix with the template $\langle 001 \rangle$ perpendicular to the surface of the tape-cast sheet. The tapes were dried, cut, and about 60 tape layers were laminated at 70°C and 200 MPa for 1 h. Samples were cut to approximately 7.5 mm × 7.5 mm × 3 mm. Samples were heated to 600°C in flowing air to remove the organic binder, followed by cold isostatic pressing (CIP) at 200 MPa for 1 min.

Tape cast samples were wrapped in a platinum foil, embedded in a 2.5% by mole fraction-excess PbO-calcined PMN–28PT coarse powder (aggregate size 50–100 μm), and placed in a covered crucible for sintering. Samples were heated in flowing O_2 (0.2 L/min) at 15°C/min to 1150°C for 10 h. The densities of the sintered samples were measured by the Archimedes method.

Random ceramic PMN–28PT samples necessary for pole figure correction and comparison with textured ceramic EBSD data were prepared by uniaxial pressing of the calcined matrix powder, followed by CIP at 200 MPa for 1 min. Samples were wrapped in a platinum foil, embedded in stoichiometric PMN–28PT powder, and sintered at 15°C/min to 1150°C for 1 h in flowing O_2 (0.2 L/min).

Textured samples for XRD Lotgering analysis, stereographic analysis, XRD rocking curve, and EBSD analysis were cut perpendicular to the $\langle 001 \rangle$ texture axis. All random and textured samples were polished to at least 6 μm. Samples for stereographic analysis and EBSD were polished to 0.02 μm with colloidal silica for at least 2 h.

Stereographic analysis was performed on a textured sample that was also thermally etched (900°C, 30 min) after polishing. ImageJ software (v. 1.32j, National Institute of Health) was used to determine the area fraction of textured grains. Five separate areas were analyzed for this calculation and averaged.

XRD pole figures were measured using a four-circle diffractometer (Philips Analytical, X'Pert Pro Materials Research Diffractometer, Almelo, the Netherlands) with Cu$K\alpha$ radiation. Scans were performed using the 002 and 111 Bragg peaks. Pole figures were measured at $2\theta = 45.18°$ and $2\theta = 38.86°$, respectively, in increments of $\Delta\psi = 3°$ and $\Delta\phi = 5°$ in the ranges of $0° \le \psi \le 69°$ and $0° \le \phi \le 360°$, with a measuring time per point of 8 s, where ψ is the tilt angle and ϕ is the azimuthal angle. Data were corrected for defocus effects by dividing the textured pole figure data by the normalized intensity of a similar scan of a randomly oriented PMN–28PT sample.

XRD rocking curve measurements were performed using the 002 Bragg peak ($2\theta = 45.18°$) of textured PMN–28PT using a standard X-ray diffractometer with CuK_α radiation (Scintag Inc., PAD V, Cupertino, CA). The range of specimen tilt, ω, was $-20°$ to $+20°$, the step size was 0.25°, and the count time was 10 s. Rocking curve data were corrected, using the TexturePlus software program,[22] to eliminate background, defocus, and absorption effects, and then fitted with the March–Dollase equation. The data collection consisted of a relatively low noise scan over the Bragg peak from the textured planes (e.g., 002, typical time about 10 min), followed by a θ scan with the detector set at the center of the Bragg peak, with a typical duration of 30–60 min. The software analysis with TexturePlus was very brief, and fitting with the March–Dollase equation was performed with a commercial package in a few minutes. For Lotgering analysis, XRD scans were performed using the same diffractometer with a 2θ range from 20° to 50°, a step size of 0.02°, and a count time of 0.5 s.

A JSM model scanning electron microscope (JEOL, Tokyo, Japan) at 20 kV was used as a base for EBSD measurements. Charging was minimized by coating the majority of the sample surface and the surrounding area with conducting silver paint. The EBSD hardware and software used in this work were from TexSEM Laboratories (Provo, Utah). The electron beam scans across the sample surface to obtain the orientation information from the spot where the beam is pointing. The software (OIM v. 2.5) analyzes the Kikuchi pattern in the digital image at every step and automatically indexes the data to preset crystal structure and phase information (PMN–28PT phase, m3m cubic structure, lattice parameter = 40.1 nm). Grain orientation maps, pole figures, and rocking curve data were generated from the collected orientation data. For the EBSD rocking curve data, orientation data from three separate areas of similar size from the sample surface were collected and averaged to improve sampling statistics.

The March–Dollase function, Eq. (1), was used to quantify the texture distributions from the XRD rocking curve and EBSD data.[23] $F(f,r,\omega)$, the fiber texture function in multiples of random distribution (MRD), is given by

$$F(f,r,\omega) = f\left(r^2\cos^2\omega + \frac{\sin^2\omega}{r}\right)^{-3/2} + (1-f) \quad (1)$$

where ω is the angle between the texture axis (sample normal) and the scattering vector, f is the volume fraction of the oriented material, r is the degree of orientation of the oriented material, and $(1-f)$ is the volume fraction of unoriented material with

$r = 1$. The r parameter characterizes the width of the texture (orientation) distribution. For a random sample, $r = 1$ and for a perfectly textured sample of tabular grains $r = 0$.

III. Results

The microstructures of the fully dense textured PMN–28PT polished surface ⊥ ⟨001⟩ texture axis (also the surface parallel to the top surface of the tape-cast sheet) and of a fracture surface // ⟨001⟩ texture axis (also the surface perpendicular to the top surface of the tape cast sheet) are shown in Figs. 1(a) and (b), respectively. The figures show large, textured grains surrounded by finer matrix grains. The size of the textured grains varies from 25 μm to 50 μm, while the matrix grains are 4–6 μm.

Pole figures and pole density plots of the (002) and (111) planes from the four circle diffractometer are shown in Figs. 2(a)–(d). Both the (002) and (111) pole figures are axisymmetric, showing that the material is fiber textured and there is no in-plane preferential orientation. The full-width at half-maximum (FWHM) is 14° for the (002) pole figure. For the (111) pole figure, the intensity is a maximum at about 56° from the sample normal, which is very close to the theoretical angle of 54.7° between (001) and (111). From the (111) plot, it is possible to see the difference in intensity for different ϕ values (for $\psi = 56°$) as the sample is rotated.

Figure 3 shows the XRD scans of randomly oriented and fiber-oriented PMN–28PT. To estimate the ⟨001⟩ texture factor, we use the Lotgering method[24]:

$$f_{(00l)} = \frac{P_{(00l)} - P_0}{1 - P_0} \tag{2}$$

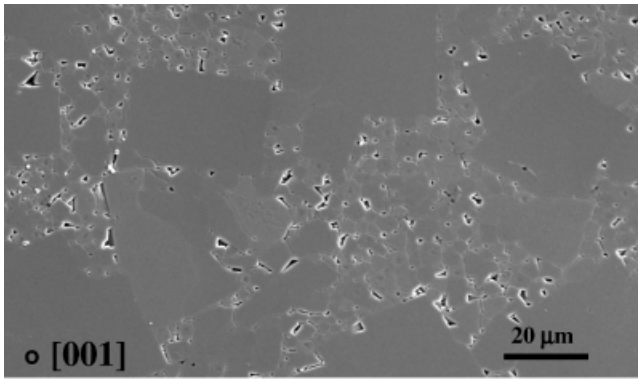

(a)

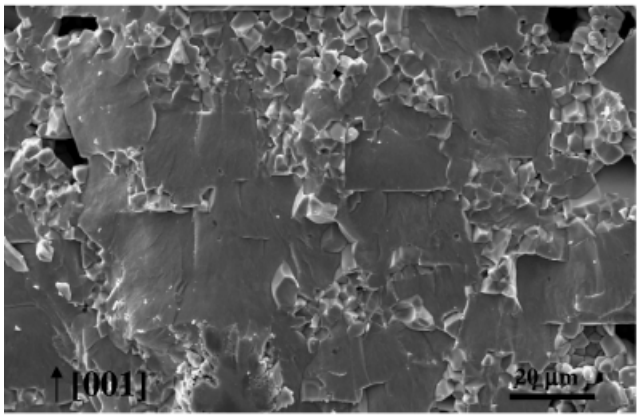

(b)

Fig. 1. Microstructures of fiber-textured lead magnesium niobate–lead titanate (PMN–28PT). (a) Scanning electron microscope (SEM) image of a polished and etched surface ⊥ ⟨001⟩ texture axis (surface parallel to top surface of the tape-cast sheet) and (b) SEM image of a fracture surface //⟨001⟩ texture axis (surface perpendicular to top surface of the tape-cast sheet).

$$\text{where } P_{(00l)} = \frac{\sum I_{(00l)}}{I_{(hkl)}} \text{ and } P_0 = \frac{\sum I_{0(00l)}}{I_{0(hkl)}} \tag{3}$$

$\sum I_{(00l)}$ is the summation of the XRD peak intensities of all the 00l peaks (i.e., 001, 002 …) in the textured PMN–28PT sample pattern. $\sum I_{(hkl)}$ is the summation of the peak intensities of all hkl peaks that appear in the XRD pattern. $\sum I_{0(00l)}$ and $\sum I_{0(hkl)}$ are summations of the XRD peak intensities for a randomly oriented sample. The f factor was calculated for a 2θ scan from 20° to 50°. The calculated f describes the fraction of texture defined by the surface area that was characterized by XRD. The Lotgering factor, f, is considered to be an estimate of the degree of orientation in the textured material. The Lotgering factor, f, of the textured PMN–28PT was calculated to be 0.74.

Stereographic analysis of the polished surface resulted in a calculated texture fraction (based on area) of 0.68 ± 0.03. Grains significantly larger than the matrix grains (i.e., $d > 10$ μm) were classified as textured grains and their area was evaluated.

XRD rocking scan data and the fit of the average of the +ω and −ω intensity data to the March–Dollase equation are shown in Figs. 4(a) and (b), respectively. The FWHM value is 13.9° for this textured material. Figure 4(b) shows that the fit of the March–Dollase equation to the rocking curve data is very good; it resulted in $f = 0.69$ and $r = 0.29$. The FWHM of the rocking curve and the pole figure are quantitatively in agreement.

The EBSD inverse pole figure maps of the textured ceramic and random ceramic are shown in Figs. 5(a) and (b), respectively. These maps of the EBSD data show the unique orientation of all of the grains in the selected areas of the ceramics. From Fig. 5(b), it is clearly shown that the larger, textured grains have ⟨001⟩-preferred orientation. The inverse pole figures of orientation data from a selected area in the random sample, an area from the only the matrix grains in the textured sample, and a selected area of the textured sample including matrix and textured grains are shown in Figs. 6(a)–(c), respectively. From these figures, we can see that there is no preferred orientation for the random sample or for the matrix grains of the textured sample (Figs. 6(a) and (b)), and that the ⟨001⟩ is the preferred orientation of the cubic textured sample (Fig. 6(c)). The 001 and 111 pole figures derived from stereographic projections of the EBSD orientation data also show the random orientation of the untextured sample in Fig. 7(a) and the ⟨001⟩ preferred orientation of the textured sample in Fig. 7(b). In Fig. 7(b), the maximum intensity of the 111 pole figure is about 50° from the center, which is close to the theoretical angle of 54.7°, between 001 and 111. The March–Dollase equation was fitted to the 001 pole figure data from the textured sample, which resulted in $f = 0.60$ and $r = 0.22$.

IV. Discussion

Table I compares the f, r, and FWHM values for the different texture analysis techniques examined in this paper. The collection area from which information for texture quality was obtained for each technique is also reported in Table I. The 95% confidence interval for the stereographic analysis and the March–Dollase fit to the XRD rocking curve and EBSD intensity data are shown for both r and f values.

The intensity data from each of the techniques were from surface grains. For XRD, the penetration depth (≈6.7 μm) of 99% of the X-ray intensity was approximately the same as the matrix grain size (however, half of these intensity data were retrieved from the first 1 μm of penetration depth). X-ray penetration depth was calculated from the mass attenuation coefficient of PMN–28PT (calculated to be 182.1 cm^2/g), the theoretical density of PMN–28PT (≈8.1 g/cm^3), and the Bragg angle ($2\theta = 45.18°$).[25] For EBSD analysis, diffraction patterns only from the surface grains were collected, as the maximum penetration depth was ≈40 nm.[26,27] Therefore, texture quality information calculated from these techniques can be directly

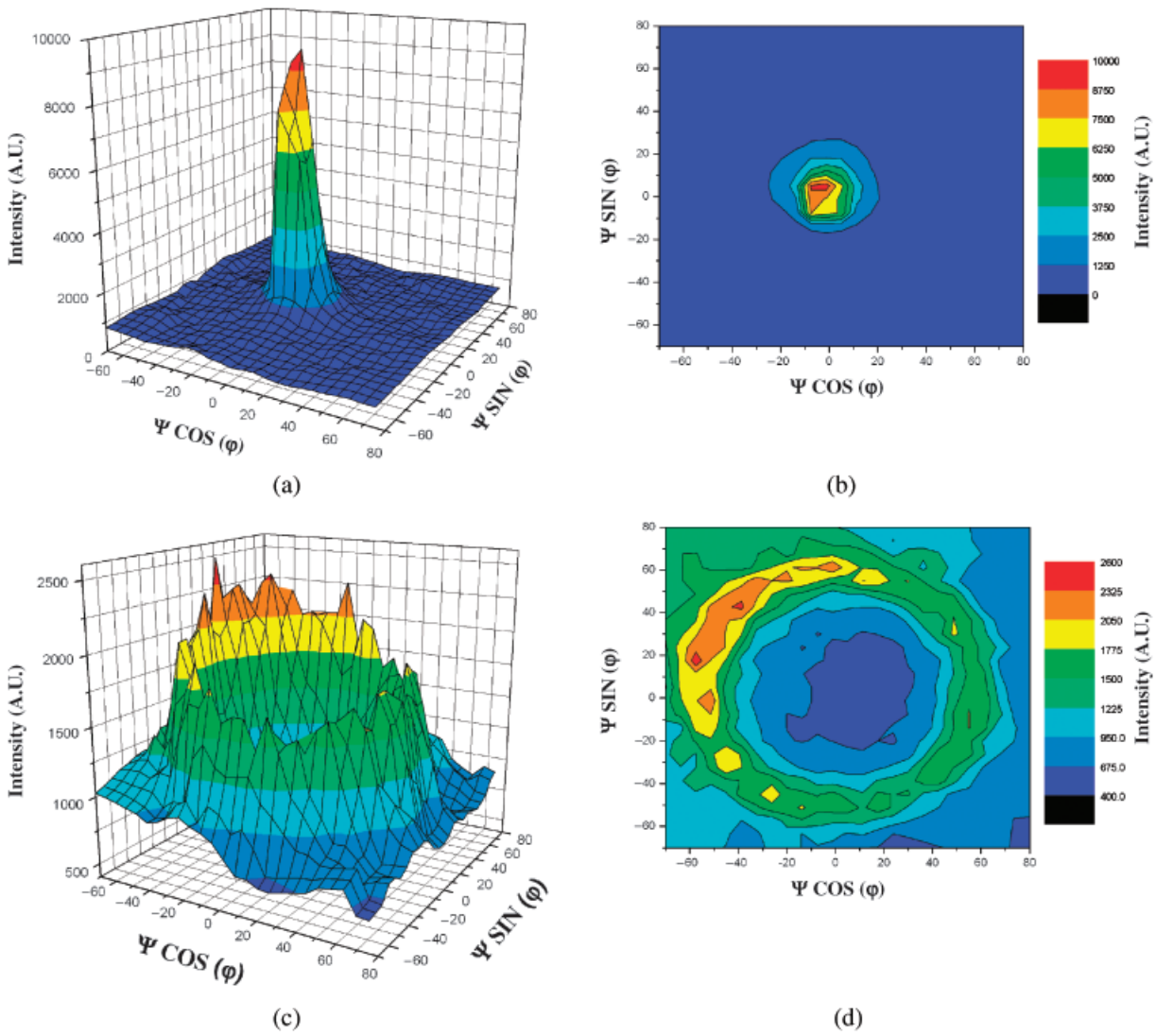

Fig. 2. (a) X-ray diffraction (XRD) pole figure of the 002 (b) XRD pole density plot of the 002 (c) XRD pole figure of the 111 (d) XRD pole density plot of the 111 plotted on a linear intensity scale in arbitrary units.

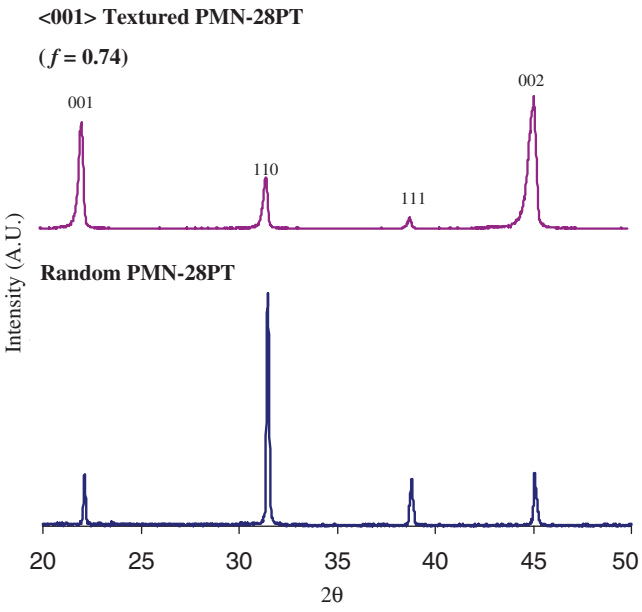

Fig. 3. X-ray diffraction (XRD) θ–2θ scan of fiber-textured lead magnesium niobate–lead titanate (PMN–28PT) and randomly oriented PMN–28PT.

compared because the intensity data, although collected over different-sized areas, were all collected from the surface grains.

The FWHM value, which measures the sharpness of the texture, was very similar for each of the techniques used (within 0.4°). This is important because the method with which the intensity data was collected was very different for each of the techniques, but the data are all quantitatively in agreement.

The March–Dollase equation considers the texture of the whole sample as being due to two populations of grains: a textured fraction, f, with orientation parameter, r, and a randomly distributed fraction $(1-f)$, where $r = 1$. The fraction of large, textured grains used for the determination of volume fraction, f, for stereographic analysis was quantitatively in agreement with f calculated from the fit of the March–Dollase equation to the XRD rocking curve and EBSD intensity data. EBSD inverse pole figure analysis on the untextured (matrix) grains in the textured sample (Fig. 6(b)) showed that the matrix region of the textured sample is indeed randomly oriented. The agreement of these data demonstrated the usefulness of fitting the March–Dollase equation to intensity data to quantify the two populations of grains and to characterize the textured fraction with an orientation parameter.

For EBSD, stereographic analysis, and rocking curve analysis, f is a measure of the volume fraction of textured material; however, for Lotgering analysis, f represents a texture quality factor and thus cannot be directly compared with the other techniques. The Lotgering factor achieved in this study is similar

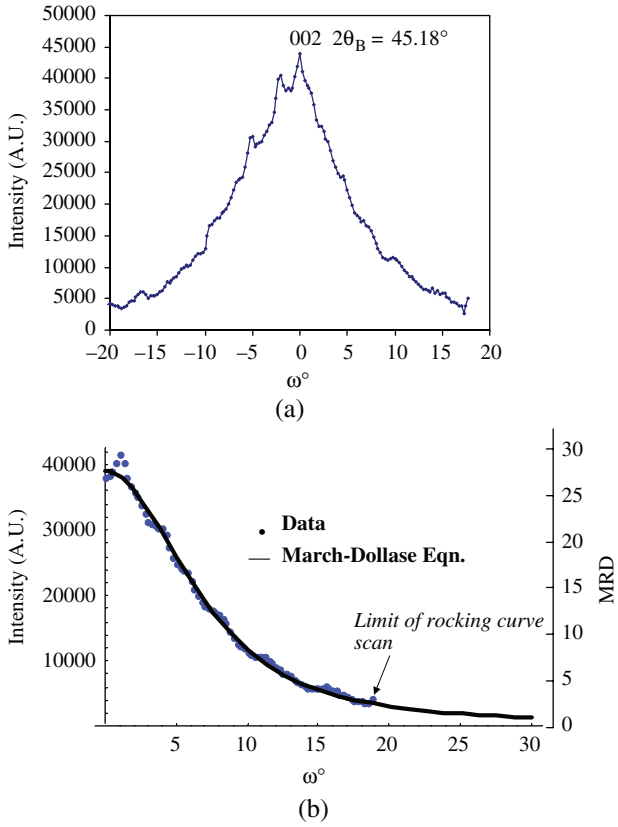

Fig. 4. (a) Corrected 002 rocking curve data for textured lead magnesium niobate–lead titanate (PMN–28PT) with full-width at half-maxima = 13.9° and (b) X-ray diffraction rocking curve data fit with the March–Dollase equation with $f = 0.69$ and $r = 0.29$.

to those reported by texturing PMN–PT by a similar process.[10] Although no information about the distribution of texture orientation is obtained from the Lotgering technique, it showed semi-quantitatively that the material is textured, and Lotgering analysis was a time-efficient technique used to show texture.

In contrast, XRD rocking curve collection and analysis described the texture quality comprehensively with f, r, and FWHM values. However, this technique also has its limitations. For samples with a wider orientation distribution, a higher 2θ Bragg peak in the same orientation as the texture axis is needed to collect a wider range of ω and fit the March–Dollase equation to the corrected data. In this material, the ω range was limited to about $\pm 20^\circ$ ω for a rocking curve on the 002 Bragg peak at $2\theta = 45.18^\circ$ using a standard θ–2θ powder diffractometer. The sample dimensions are also an important consideration. The scatter in Fig. 4(a) could be decreased with a larger sampling area, but in general ≈ 1 cm^2 is necessary for this technique.[22,28] Despite the scatter in the rocking curve data, the fit of the March–Dollase equation to the data was quite good, with a $\chi^2 = 0.99$. The f and r values derived from this fit had very narrow confidence intervals, as can be seen in Table I. The XRD rocking curve data fitted with the March–Dollase equation are the preferred way to measure texture in the textured materials of this study due to the relative ease of measurement and the amount of texture quantification data collected from this technique.

A benefit of EBSD analysis is the visualization of the microstructure orientation through the inverse pole figure maps. The same data (pole figures, rocking curves, etc.) generated from other techniques can be obtained from a single EBSD scan. In contrast to XRD techniques, sample dimensions in EBSD analysis are usually not a consideration. However, sampling statistics are much lower compared with XRD techniques due to the difference in area analyzed (sampling area is $\approx 800\times$ greater for XRD Lotgering and XRD rocking curve analysis), even though multiple scans are used in the analysis. Scans over larger areas

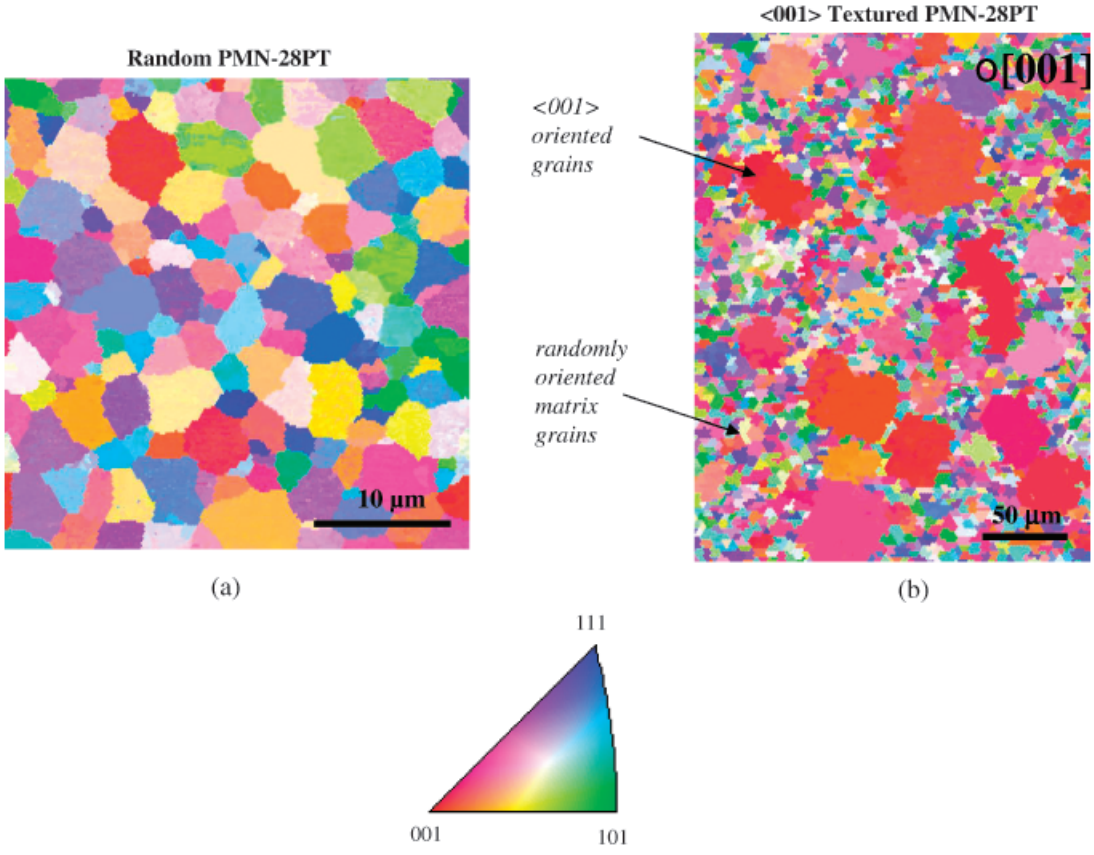

Fig. 5. Electron backscatter diffraction inverse pole figure maps using stereographic projections of (a) a randomly oriented lead magnesium niobate–lead titanate (PMN–28PT) (335 grains) and (b) fiber-textured PMN–28PT (1402 grains).

Table I. Comparison of Texture Fraction (*f*), Orientation Parameter (*r*), and FWHM in <001> Fiber-Oriented PMN–28PT for Different Texture Analysis Techniques

Analysis technique	Data collection area (mm^2)	*f*	*r*	FWHM
Lotgering method	79.4	0.74[†]	—	—
Stereographic analysis	5.0×10^{-2}	0.68±0.03	—	—
XRD rocking curve	79.4	0.69±0.02	0.29±0.004	13.9°
XRD pole figure	39.7	–	–	14°
EBSD	10.4×10^{-2}	0.60±0.11	0.22±0.02	13.6°

[†]For Lotgering analysis, *f* represents texture quality factor; XRD, X-ray diffraction; EBSD, electron backscatter diffraction; FWHM, full-width at half-maxima; *r*, March parameter.

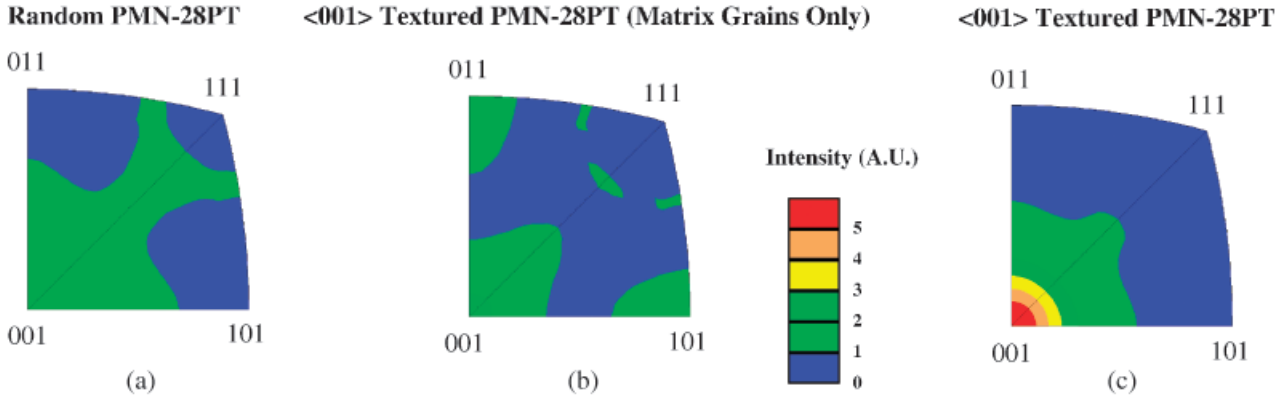

Fig. 6. 001 electron backscatter diffraction inverse pole figures using stereographic projections of (a) randomly oriented lead magnesium niobate–lead titanate (PMN–28PT) (335 grains), (b) matrix grains from fiber-textured PMN–28PT (193 grains), and (c) fiber-textured lead magnesium niobate–lead titanate (PMN–28PT) (1402 grains) plotted on a linear intensity scale in arbitrary units.

($\approx$1 mm^2) have been accomplished in previous studies on conductive samples in standard EBSD systems and on non-conductive samples in partial pressure of water vapor to limit charging, which is the limit to the area analyzed in this study.[19,26] As a result, the *f* and *r* values derived from the fit of the March–Dollase equation to the EBSD rocking curve data ($\chi^2 = 0.96$) had more broad confidence intervals, as can be seen in Table I. This might also account for the lower *f* and *r* values for this technique. Furthermore, sample preparation and data collection for EBSD analysis can be very time consuming.

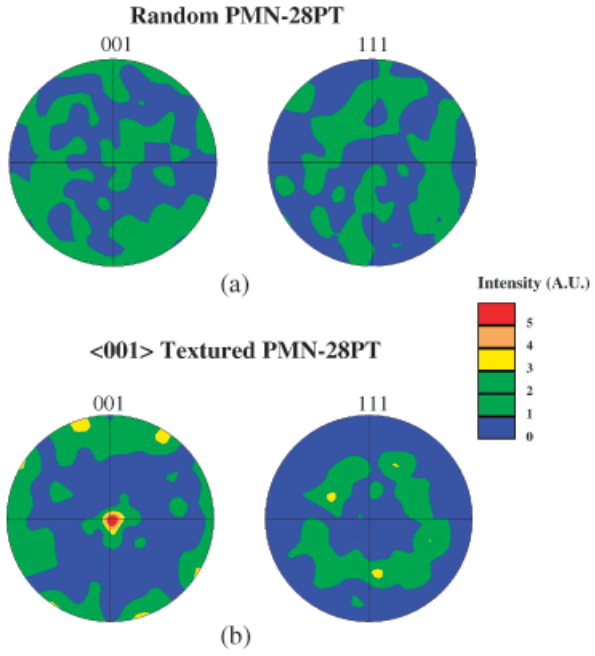

Fig. 7. 001 and 111 electron backscatter diffraction pole figure plots using stereographic projections of (a) randomly oriented lead magnesium niobate–lead titanate (PMN–28PT) (335 grains) and (b) fiber-textured PMN–28PT plotted (1402 grains) plotted on a linear intensity scale in arbitrary units.

V. Summary

Textured PMN–PT prepared by the TGG process has been shown to possess a significant fraction of the piezoelectric properties of the single crystal. Until recently, characterization of texture in this material has been limited to Lotgering analysis. In this study, XRD and EBSD techniques were used to characterize the fiber texture in oriented PMN–28PT and the intensity data were fit with the March–Dollase equation to describe the texture in terms of texture fraction (*f*), and the width of the orientation distribution (*r*). Although XRD rocking curve, XRD pole figure, and EBSD data analysis gave similar *f*, *r*, and FWHM values, XRD rocking curve analysis was the most efficient and gave a complete description of texture fraction and texture orientation. XRD rocking curve analysis is the preferred approach for comprehensive texture characterization in fiber-oriented PMN–PT.

Acknowledgment

Disclaimer: The identification of any commercial product or trade name is for information only and does not imply endorsement or recommendation by the National Institute of Standards and Technology.

References

[1]J. M. Powers, M. B. Moffett, and F. Nussbaum, "Single Crystal Naval Transducer Development"; pp. 351–4 in *Proceedings of the 12th IEEE International Symposium on Applications of Ferroelectrics*, Vol. 1, Edited by S. K. Streiffer, B. Gibbons, and T. Tsurumi. Institute of Electrical and Electronics Engineers, New York, NY, 2000.

[2]S. E. Park and T. R. Shrout, "Characteristics of Relaxor-Based Piezoelectric Single Crystals for Ultrasonic Transducers," *IEEE Trans. Ultrasonics Ferroelect. Frequency Control*, **44** [5] 1140–7 (1997).

[3]S. E. Park and T. R. Shrout, "Ultrahigh Strain and Piezoelectric Behavior in Relaxor Based Ferroelectric Single Crystals," *J. Appl. Phys.*, **82** [4] 1804–11 (1997).
[4]S. G. Lee, R. G. Monteiro, R. S. Feigelson, H. S. Lee, M. Lee, and S. E. Park, "Growth and Electrostrictive Properties of $Pb(Mg_{1/3}Nb_{2/3})O_3$ Crystals," *Appl. Phys. Lett.*, **74** [7] 1030–2 (1999).
[5]K. T. Zawilski, M. C. Custodio, R. C. DeMattei, S. G. Lee, R. G. Monteiro, H. Odagawa, and R. S. Feigelson, "Segregation During the Vertical Bridgman Growth of Lead Magnesium Niobate-Lead Titanate Single Crystals," *J. Crystal Growth*, **258** [3–4] 353–67 (2003).
[6]E. M. Sabolsky, A. R. James, S. Kwon, S. Trolier-McKinstry, and G. L. Messing, "Piezoelectric Properties of ⟨001⟩ Textured $Pb(Mg_{1/3}Nb_{2/3})O_3$-$PbTiO_3$ Ceramics," *Appl. Phys. Lett.*, **78** [17] 2551–3 (2001).
[7]E. M. Sabolsky, S. Kwon, E. Suvaci, A. R. James, G. L. Messing, and S. Trolier-McKinstry, "Dielectric and Electromechanical Properties of ⟨001⟩ -Textured $(0.68)Pb(Mg_{1/3}Nb_{2/3})O_3$-$(0.32)PbTiO_3$"; pp. 393–6 in *Proceedings of the 2000 IEEE International Symposium on Applications of Ferroelectrics*, Vol. 1, Edited by S. K. Streiffer. Institute of Electrical and Electronics Engineers, New York, NY, 2000.
[8]E. M. Sabolsky, G. L. Messing, and S. Trolier-McKinstry, "Kinetics of Templated Grain Growth of $0.65Pb(Mg_{1/3}Nb_{2/3})O_3$–$0.35PbTiO_3$," *J. Am. Ceram. Soc.*, **84** [11] 2507–13 (2001).
[9]E. M. Sabolsky, S. Trolier-McKinstry, and G. L. Messing, "Dielectric and Piezoelectric Properties of ⟨001⟩ Fiber-Textured $0.675Pb(Mg_{1/3}Nb_{2/3})O_3$–$0.325PbTiO_3$ Ceramics," *J. Appl. Phys.*, **93** [7] 4072–80 (2003).
[10]S. Kwon, E. M. Sabolsky, G. L. Messing, and S. Trolier-McKinstry, "High Strain, ⟨001⟩ Textured $0.675Pb(Mg_{1/3}Nb_{2/3})O_3$–$0.325PbTiO_3$ Ceramics: Templated Grain Growth and Piezoelectric Properties," *J. Am. Ceram. Soc.*, **88** [2] 312–7 (2005).
[11]G. L. Messing, S. Trolier-McKinstry, E. M. Sabolsky, C. Duran, S. Kwon, B. Brahmaroutu, P. Park, H. Yilmaz, P. W. Rehrig, K. B. Eitel, E. Suvaci, M. Seabaugh, and K. S. Oh, "Templated Grain Growth of Textured Piezoelectric Ceramics," *Critical Rev. Solid State Mater. Sci.*, **29**, 45–96 (2004).
[12]M. Allahverdi, A. Hall, R. Brennan, M. E. Ebrahimi, N. M. Hagh, and A. Safari, "An Overview of Rapidly Prototyped Piezoelectric Actuators and Grain-Oriented Ceramics," *J. Electroceram.*, **8** [2] 129–37 (2002).
[13]T. Kimura, Y. Miura, and K. Fuse, "Texture Development in Barium Titanate and PMN-PT Using Hexabarium 17-Titanate Heterotemplates," *Int. J. App. Ceram. Technol.*, **2** [1] 15–23 (2005).
[14]S. W. Sun, X. M. Pan, P. C. Wang, L. H. Zhu, Q. W. Huang, D. L. Li, and Z. W. Yin, "Fabrication and Electrical Properties of Grain-Oriented $0.7Pb(Mg_{1/3}Nb_{2/3})O_3$–$0.3PbTiO_3$ Ceramics," *Appl. Phys. Lett.*, **84** [4] 574–6 (2004).
[15]J. L. Jones, E. B. Slamovich, and K. J. Bowman, "Critical Evaluation of the Lotgering Degree of Orientation Texture Indicator," *J. Mater. Res.*, **19** [11] 3414–22 (2004).
[16]M. M. Seabaugh, M. D. Vaudin, J. P. Cline, and G. L. Messing, "Comparison of Texture Analysis Techniques for Highly Oriented α-Al_2O_3," *J. Am. Ceram. Soc.*, **83** [8] 2049–54 (2000).
[17]M. M. Seabaugh, G. L. Messing, and M. D. Vaudin, "Texture Development and Microstructure Evolution in Liquid-Phase-Sintered α-Alumina Ceramics Prepared by Templated Grain Growth," *J. Am. Ceram. Soc.*, **83** [12] 3109–16 (2000).
[18]H. Yilmaz, G. L. Messing, and S. Trolier-McKinstry, "(Reactive) Templated Grain Growth of Textured Sodium Bismuth Titanate ($Na_{1/2}Bi_{1/2}TiO_3$-$BaTiO_3$) Ceramics–I. Processing," *J. Electroceram.*, **11** [3] 207–15 (2003).
[19]A. Khan, D. T. Carpenter, A. M. Scotch, H. M. Chan, and M. P. Harmer, "Electron Backscatter Diffraction Analysis of $Pb(Mg_{1/3}Nb_{2/3})O_3$–35mol% $PbTiO_3$ Single Crystals Grown by Seeded Polycrystal Conversion," *J. Mater. Res.*, **16** [3] 694–700 (2001).
[20]G. L. Messing, S. Trolier-McKinstry, and K. Watari, "Anisotropically Shaped SrTiO3 Single Crystal Particles"; U.S. Patent No. 6,514,476, Penn State Research Foundation, University Park, PA, 2003.
[21]K. Watari, B. Brahmaroutu, G. L. Messing, S. Trolier-McKinstry, and S. C. Cheng, "Epitaxial Growth of Anisotropically Shaped, Single-crystal Particles of Cubic $SrTiO_3$," *J. Mater. Res.*, **15** [4] 846–9 (2000).
[22]M. D. Vaudin "TexturePlus," National Institute of Standards and Technology, Ceramics Division, Gaithersburg, MD. (Program available by written request (E-mail: mark.vaudin@nist.gov) or on the World Wide Web (http://www.ceramics.nist.gov/webbook/TexturePlus/texture.htm))
[23]W. A. Dollase, "Correction of Intensities for Preferred Orientation in Powder Diffractometry - Application of the March Model," *J. App. Crystallography*, **19**, 267–72 (1986).
[24]F. K. Lotgering, "Topotactical Reactions with Ferrimagnetic Oxides Having Hexagonal Crystal Structures-I," *J. Inorg. Nucl. Chem.*, **9**, 113–23 (1959).
[25]B. D. Cullity, *Elements of X-ray Diffraction*, 555 pp Addison-Wesley Publishing Company Inc, Reading, MA, 1978.
[26]D. Dingley, "Progressive Steps in the Development of Electron Backscatter Diffraction and Orientation Imaging Microscopy," *J. Microsc.*, **213** [3] 214–24 (2004).
[27]D. J. Dingley and V. Randle, "Review. Microtexture Determination by Electron Back-scatter Diffraction," *J. Mater. Sci.*, **27**, 4545–66 (1992).
[28]M. D. Vaudin, M. W. Rupich, M. Jowett, G. N. Riley, and J. F. Bingert, "A Method for Crystallographic Texture Investigations Using Standard X-ray Equipment," *J. Mater. Res.*, **13** [10] 2910–9 (1998). □